Available online at https://link.springer.com/journal/42241
http://www.jhydrodynamics.com
Journal of Hydrodynamics, 2021
https://doi.org/10.1007/s42241-021-0067-z

Optimization of the roll motion of box-shaped hull section with anti-rolling sloshing tanks and fins in beam waves *

Xin-wang Liu[1], Wei-wen Zhao[1], De-cheng Wan[1, 2]
1. *Computational Marine Hydrodynamics Lab (CMHL), School of Naval Architecture, Ocean and Civil Engineering, Shanghai Jiao Tong University, Shanghai 200240, China*
2. *Ocean College, Zhejiang University, Zhoushan 316021, China*

(Received July 29, 2021, Revised August 2, 2021, Accepted August 3, 2021, Published online August 20, 2021)

Abstract: With the development of ocean engineering and demand for safety of the ship and offshore structures, the transportation and storage of liquid have become an important issue nowadays. Furthermore, in order to improve the hydrodynamic performances of the ship and offshore structures, the anti-rolling liquid tanks are often taken into consideration. The internal-external coupling flow effect is vital for the ship and liquid tank designs, especially when the external wave frequency is close to the natural frequency of liquid tanks with a certain filling ratio, large amplitude motions may occur, which is dangerous to some extent. In this paper, the simulation-based-design method is introduced at first, and the verification of the numerical calculation of internal-external coupling flow with liquid tanks is done then. Finally, the filling ratio of the anti-rolling liquid tank and the installation angle of the anti-rolling fins are optimized to reduce the roll motion amplitude of the hull section to the greatest extent under the combined action of the two anti-rolling devices. Optimization results show that the roll motion amplitude of box-shaped hull section can be successfully reduced by reasonably designing the two anti-rolling devices, which can be a reference to the future design of the fishing ship and other ships with anti-rolling devices.

Key words: Tank sloshing, anti-rolling fin, ship motion in waves, ship hydrodynamic optimization

Introduction

With huge development of ocean engineering and demand for safety of the ship and offshore structures, the transportation and storage of liquid, such as liquefied natural gas (LNG), have become a crucial issue these days. Furthermore, in order to improve the hydrodynamic performances of the ship and offshore structures, the anti-rolling liquid tanks are often taken into consideration. Quite different from the ships without liquid tanks, the motion of ship with liquid tanks is caused by external wave excitation and internal sloshing both. This kind of internal-external coupling flow effect is vital for the ship and tank designs. In particular, when the external wave frequency is close to the natural frequency of liquid tanks with a certain filling ratio, large amplitude motions may occur, which is dangerous to some extent. Therefore, it's essential to study the coupling effect of ship motion with liquid tanks, in order to ensure the safety of the transportation and storage of liquid, and improve the hydrodynamic performances of the ship and offshore structures.

Sloshing tanks have been studied in earlier times before the ship motions in waves coupled with sloshing tanks. Mikelis et al.[1] solved liquid cargo sloshing flow using a two-dimensional finite difference method compared with the model test results, leading to many researches focusing on the internal-external flow coupling effect. Rognebakke and Faltinsen[2] solved two-dimensional rectangular hull section in regular waves using potential theory, and pointed out that the sloshing flow is dominated by external wave frequency. However, the motions of ship and sloshing liquid in tank were solved seperately. Newman[3] started to use WAMIT to solve the motions of ship and sloshing liquid in tank as a whole, that is, the internal fluid in tank is regarded as an extension of the external fluid outside the tank, which is a very important strategy that can also be implemented in viscous-flow based solvers. For instance,

* Projects supported by the National Key Research and Development Program of China (Grant Nos. 2019YFB1704200, 2019YFC0312400), the National Natural Science Foundation of China (Grant No. 51879159).
Biography: Xin-wang Liu (1995-), Male, Ph. D. Candidate,
E-mail: huhgf670@163.com
Corresponding author: De-cheng Wan,
E-mail: dcwan@sjtu.edu.cn

SOLA method[4] was first applied to simulate a three-dimensional sloshing flow. Furthermore, Jiang et al.[5], Saripilli and Sen[6] simulated the internal field in tank by a viscous-flow-based computational fluid dynamics (CFD) open source toolbox OpenFOAM, and the external field by potential flow theory. Shen and Wan [7] realized the fully-coupled method of ship motion and tank sloshing through the viscous-flow-based solver naoe-FOAM-SJTU on the KVLCC2 ship model coupled with two LNG tanks. However, few researches are found to do the optimization of the ship roll motion in beam waves with sloshing tanks and other anti-rolling devices, such as anti-rolling fins.

In this paper, the simulation-based-design method is first introduced, and the verification of the numerical calculation of internal-external coupling flow with liquid tanks is then done. Finally, the filling ratio of the anti-rolling liquid tank and the installation angle of the anti-rolling fins are optimized in this paper, in order to reduce the roll motion amplitude of the hull section to the greatest extent under the combined action of the two anti-rolling devices.

1. Optimization methods

1.1 *Hydrodynamic performance evaluation*

For the hydrodynamic performance evaluation of the hull with sloshing tanks, the viscous-flow-based solver naoe-FOAM-SJTU[7] is used in this paper.

The URANS equations are used to address the unsteady incompressible viscous flow in naoe-FOAM-SJTU solver. The Navier-Stokes equations include the continuity and the momentum equations, considering dynamic deformation mesh, the governing equations are:

$$\nabla \cdot \boldsymbol{U} = 0 \tag{1}$$

$$\frac{\partial \rho \boldsymbol{U}}{\partial t} + \nabla \cdot [\rho(\boldsymbol{U} - \boldsymbol{U}_g)\boldsymbol{U}] = -\nabla p_d - \boldsymbol{g} \cdot \boldsymbol{x} \nabla \rho + \nabla(\mu_{\text{eff}} \nabla \boldsymbol{U}) + f_\sigma \tag{2}$$

where $\boldsymbol{U}$ is the velocity field, $\boldsymbol{U}_g$ is the velocity of grid node, ρ is the mixed density with water and air, $p_d = p - \rho \boldsymbol{g} \cdot \boldsymbol{x}$ is the dynamic pressure, p is the total pressure, $\mu_{\text{eff}} = \rho(\nu + \nu_t)$ is the effective dynamic viscosity, in which ν and ν_t are kinematic viscosity and eddy viscosity respectively, and f_σ is the surface tension term in the two-phase model. The choice of turbulence model is the k-ω SST model.

The free surface is captured by volume of fluid (VOF) method[8] with artificial bounded compression techniques. Each of the two phases in VOF method is considered to have a separately defined volume fraction α, indicating the relative proportion of fluid in each cell, and its value is always between 0 and 1, that is:

$$\alpha = 0 \quad \text{air} \tag{3a}$$

$$0 < \alpha < 1 \quad \text{interface} \tag{3b}$$

$$\alpha = 1 \quad \text{water} \tag{3c}$$

In order to capture the sharp interface and ensure conservation and boundedness, an extra term is added into VOF transport equation shown below

$$\frac{\partial \alpha}{\partial t} + \nabla \cdot [\alpha(\boldsymbol{U} - \boldsymbol{U}_g)] + \nabla \cdot [\alpha(1-\alpha)\boldsymbol{U}_r] = 0 \tag{4}$$

where $\boldsymbol{U}_r$ is the velocity field used to compress the interface. It is normal to the interface so it does not affect the flow along interface, and the description of $\boldsymbol{U}_r$ is given below

$$\boldsymbol{U}_r = \boldsymbol{n}_f \min\left\{ c_\alpha \frac{|\varphi|}{|\boldsymbol{S}_f|}, \max\left(\frac{|\varphi|}{|\boldsymbol{S}_f|} \right) \right\} \tag{5}$$

where φ is the face volume flux, $\boldsymbol{n}_f$ is the normal vector of cell face, and $\boldsymbol{S}_f$ is the area vector of cell face parallel to vector $\boldsymbol{n}_f$. A recommended setting of c_α is equal to 1 to maintain the sharp interface. Besides, the surface tension term f_σ in Eq. (2) is defined as

$$f_\sigma = \sigma \kappa \nabla \alpha \tag{6}$$

where σ is the surface tension coefficient, which is chosen to be 0.07 kg/s^2, and κ is the curvature of surface interface, which can be calculated by α

$$\kappa = -\nabla \cdot \left(\frac{\nabla \alpha}{|\nabla \alpha|} \right) \tag{7}$$

A fully 6 degrees-of-freedom (DOF) module with bodies is implemented. Two coordinate systems are used to solve 6DOF equations. The six degrees of freedom are defined as the translation and rotation angles of the hull, namely $(x_1, x_2) = (x, y, z, \varphi, \theta, \psi)$, representing motions of surge, sway, heave, roll, pitch and yaw, respectively. $(v_1, v_2) = (u, v, w, p, q, r)$ are

the linear and angular velocities in the earth-fixed coordinate system, which can be transformed to the body-fixed coordinate system by the following equations:

$$v_1 = J_1^{-1}\dot{x}_1, \quad v_2 = J_2^{-1}\dot{x}_2 \tag{8}$$

where J_1, J_2 are transformation matrices based on Euler angle. The forces and moments are projected into the earth-fixed system in the following way:

$$F = (X,Y,Z) = J_1^{-1}F_e, \quad M = (K,M,N) = J_2^{-1}M_e \tag{9}$$

F and M with (or without) subscript e means the forces and moments in the earth (or body)-fixed system. The linear and angular acceleration in body-fixed system can be given as follows:

$$\dot{u} = \frac{X}{m} + vr - wq + x_g(q^2 + r^2) - y_g(pq - \dot{r}) - z_g(pr + \dot{q}) \tag{10a}$$

$$\dot{v} = \frac{Y}{m} + wp - ur + y_g(r^2 + p^2) - z_g(qr - \dot{p}) - x_g(qp + \dot{r}) \tag{10b}$$

$$\dot{w} = \frac{Z}{m} + uq - vp + z_g(p^2 + q^2) - x_g(rp - \dot{q}) - y_g(rp + \dot{p}) \tag{10c}$$

$$\dot{p} = \frac{1}{I_x}\{K - (I_z - I_y)qr - m[y_g(\dot{w} - uq + vp) - z_g(\dot{v} - wp + ur)]\} \tag{10d}$$

$$\dot{q} = \frac{1}{I_y}\{M - (I_x - I_z)rp - m[z_g(\dot{u} - vr + wq) - x_g(\dot{w} - uq + vp)]\} \tag{10e}$$

$$\dot{r} = \frac{1}{I_z}\{N - (I_y - I_x)pq - m[x_g(\dot{v} - wp + ur) - y_g(\dot{u} - vr + wq)]\} \tag{10f}$$

where m is the mass of the motion body, I_x, I_y and I_z represent the moments of the inertia on the center of rotation in three directions, X, Y, Z, K, M and N are surge, sway, heave forces and roll, pitch, yaw moments, respectively, x_g, y_g and z_g are the coordinates of the center of gravity.

The hull section motion and tank sloshing are solved as a whole, therefore only the motion of hull section needs the moving-mesh technique. In this paper, the mesh deforms according to the computation of the hull section motion given above. The position of the mesh points in the computational domain is solved by a Laplace equation with varying diffusivity

$$\nabla \cdot (\gamma \nabla \boldsymbol{x}_g) = 0 \tag{11}$$

where $\boldsymbol{x}_g$ is the displacement of mesh nodes, γ is the diffusivity field, which is determined by

$$\gamma = \frac{1}{r^2} \tag{12}$$

where r is the nearest distance between each cell center to the moving boundary.

Furthermore, the regular wave is generated at the inlet by imposing the boundary conditions of α and $\boldsymbol{U}$. The linear Stokes wave in deep water is applied for the wave maker

$$\eta = A\cos(kx - \omega_e t) \tag{13}$$

where η is the wave elevation, A is the wave amplitude, k is the wave number, and ω is the natural frequency of incident wave, while ω_e is the encounter frequency, since the box-shaped hull section does not have a forward speed, $\omega_e = \omega$ in this condition.

Although the outlet boundary condition is usually adopted to let the flux flow out, the phenomenon of wave reflection can occur near the outlet. Without a theoretically mature outlet boundary condition can be used, a wave absorbing area, which is also called sponge layer, is applied, in which the wave will decay[9] to achieve wave absorbing. The wave absorbing can be easily realized by adding an extra source term in momentum equation[10].

Fully coupled model[11] is used to do the simulation of box-shaped hull section with liquid tanks in beam waves. The approach is unified so the internal as well as external free surface is solved simultaneously. With a small-enough tunnel exists on the top of the tank, the inner space is connected with the outer space. Since the existence of the tunnel, the pressure and velocity of inner fields and outer fields

keep the same at the beginning of the simulation. Therefore, the internal fluid can be regarded as an extension of external fluid without many modifications.

Last but not least, Van Leer scheme is applied for VOF equation in OpenFOAM. The RANS and VOF transport equations are discretized by finite volume method (FVM). The PIMPLE algorithm is used to solve the coupled equation of velocity and pressure. The convection terms are approximated by a second-order TVD limited linear scheme, and the diffusion terms are approximated by a second-order central difference scheme.

1.2 *Surrogate model construction*

For the surrogate model construction module, in order to save computational costs, one alternative method is to construct a relatively simple surrogate model instead of complicated numerical analysis of a large number of sample points in order to find the relationship, which is often with strong nonlinearity, between the design variables (input) and the objective functions (output). The sample points should be selected at the beginning of the optimization procedure, and the meshes of new sample cases can be got, and the hydrodynamic evaluation can be implemented.

The sample points can be selected using different design of experiment methods, such as optimal latin hypercube sampling (OLHS) method[12-13] and Sobol method[14], by which the sample points have good uniformity and orthogonality in the whole design space.

After evaluating the hydrodynamic performance of the series of new samples, the surrogate model can be constructed. Some models are widely used such as response surface model, Kriging model and artificial neural network model[15-17]. For instance, the Kriging surrogate model expresses the relationship between the design variables and the objective functions using a stochastic Gaussian process, which is able to exploit the spatial correlation of data in order to predict the shape of the objective function based only on limited information.

Kriging exploits the spatial correlation of data in order to build interpolation, so the correlation function is a critical element. Hence, this model combines a global model and a local component

$$y(\boldsymbol{x}) = f(\boldsymbol{x}) + z(\boldsymbol{x}) \tag{14}$$

where $y(\boldsymbol{x})$ is the unknown real function, $f(\boldsymbol{x})$ is a known approximation function, and $z(\boldsymbol{x})$ is the realization of a stochastic process with mean zero, variance σ^2, and non-zero covariance. With $f(\boldsymbol{x})$ and $z(\boldsymbol{x})$, the Kriging model can be built to represent the relationship between the input variables and output variables.

The Kriging predictor is given by

$$\hat{y} = \hat{\beta} + \boldsymbol{r}^{\mathrm{T}}(\boldsymbol{x})\boldsymbol{R}^{-1}(\boldsymbol{y} - \boldsymbol{f}\hat{\beta}) \tag{15}$$

where $\hat{y}$ is an n_s-dimensional vector that contains the sample values of the response, $\boldsymbol{f}$ is a column vector of length n_s that is filled with ones when $\boldsymbol{f}$ is taken as a constant, that is $\boldsymbol{f}_{n_s\times 1} = [1,1,\cdots,1]^{\mathrm{T}} = \boldsymbol{1}$, $\boldsymbol{r}^{\mathrm{T}}(\boldsymbol{x})$ is the correlation vector of length n_s between an untried $\boldsymbol{x}$ and the sample points $\{\boldsymbol{x}^{(1)}, \boldsymbol{x}^{(2)}, \cdots, \boldsymbol{x}^{(n_s)}\}$, which is expressed as

$$\boldsymbol{r}^{\mathrm{T}}(\boldsymbol{x}) = [R(\boldsymbol{x}, \boldsymbol{x}^{(1)}), R(\boldsymbol{x}, \boldsymbol{x}^{(2)}), \cdots, R(\boldsymbol{x}, \boldsymbol{x}^{(n_s)})]^{\mathrm{T}} \tag{16}$$

In addition, the Gaussian correlation function is employed in this study to represent the spatial relation of the objective function among the samples in the design space

$$R(\boldsymbol{x}^{(i)}, \boldsymbol{x}^{(j)}) = \exp\left[-\sum_{k=1}^{n_{dv}} \theta_k \left|\boldsymbol{x}_k^{(i)} - \boldsymbol{x}_k^{(j)}\right|^2\right] \tag{17}$$

In Eq. (15), $\hat{\beta}$ is estimated by

$$\hat{\beta} = (\boldsymbol{f}^{\mathrm{T}}\boldsymbol{R}^{-1}\boldsymbol{f})^{-1}\boldsymbol{f}^{\mathrm{T}}\boldsymbol{R}^{-1}\boldsymbol{y} \tag{18}$$

The estimate of the variance $\hat{\sigma}^2$, between the underlying global model $\hat{\beta}$ and $\boldsymbol{y}$ is estimated by

$$\hat{\sigma}^2 = \frac{(\boldsymbol{y} - \boldsymbol{f}\hat{\beta})^{\mathrm{T}}\boldsymbol{R}^{-1}(\boldsymbol{y} - \boldsymbol{f}\hat{\beta})}{n_s} \tag{19}$$

where $f(\boldsymbol{x})$ is assumed to just be the constant $\hat{\beta}$.

The maximum likelihood estimates for parameters θ_k in Eq. (17) in order to fit a Kriging model, which are obtained by solving an optimization problem

$$\max_{\theta_k > 0} \Phi(\theta_k) = -\frac{n_s \ln(\hat{\sigma}^2) + \ln|\boldsymbol{R}|}{2} \tag{20}$$

where both $\hat{\sigma}^2$ and $\boldsymbol{R}$ are functions of θ_k.

While any values for θ_k create an interpolative Kriging model, the "best" Kriging model is found by

solving the k-dimensional unconstrained, nonlinear, optimization problem given above.

The accuracy of the prediction value largely depends on the distance from sample points. Intuitively speaking, the closer point $\boldsymbol{x}$ to the sample points, the more accurate is the prediction $\hat{y}$.

1.3 *Optimization algorithm*

Consider an optimization problem where there is a need to optimize one variable or a set of variables in order to maximize or minimize an output. For the single-objective optimization, many intelligent optimization algorithms are widely used to solve this kind of optimization problem, such as genetic algorithm (GA)[18] and particle swarm optimization (PSO)[19] algorithms.

An implementation of a traditional GA starts by generating N numbers of initial population of typically random chromosomes, and then evaluates the structures and allocates reproductive opportunities in a way that those chromosomes which indicate better solutions to the optimization problem are given more opportunities to reproduce than those which are poorer solutions. The goodness of a solution is typically defined with respect to the current population.

That is to say, parents are then chosen utilizing the competitive selection method via selection, crossover and mutation operators borrowed from natural genetics. After blend of this new population with previous population, an again sorting is implemented. Among the present population, which has a more population number than the initial one, the N top members are selected for the next generation. The criteria of population selection for the generation update can be first top front. This process leads to the evolution of populations of individuals that are better suited to the environment than the individuals that they were created from, just as in real natural adaptation. In order to validate the GA used in this paper, a mathematical function is tested to find its global minimum.

Proposed by Ackley[20], the Ackley's function is a non-convex function used as a test problem for optimization algorithms. In its two-dimensional form, shown as Fig. 1, it is characterized by a nearly flat outer region, and a large trough at the center. Therefore, it gives a risk for optimization algorithms, particularly hill-climbing algorithms, to be easily trapped in any one of its local minima.

On a two-dimensional domain $[-5,5]\times[-5,5]$, it is defined by

$$f(x,y) = -20\mathrm{e}^{-0.2\sqrt{0.5(x^2+y^2)}} - \mathrm{e}^{0.5(\cos 2\pi x+\cos 2\pi y)} + \mathrm{e} + 20 \tag{21}$$

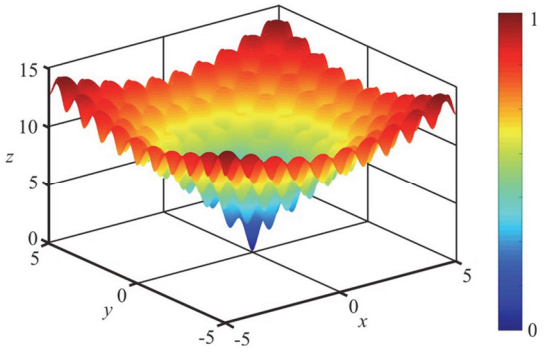

Fig. 1 (Color online) Graph of Ackley's function

Its global minimum point is

$$f(0,0) = 0 \tag{22}$$

Setting the Ackley's function as the objective function to find its minimum, the convergence of GA is shown in Fig. 2, and the found optimum point through 100 repeated times is

$$f(-2.50\times10^{-7}, 2.19\times10^{-6}) = 6.22\times10^{-6} \tag{23}$$

It can be easily seen from Fig. 2 that the GA can be successfully used in the single-objective optimization problems.

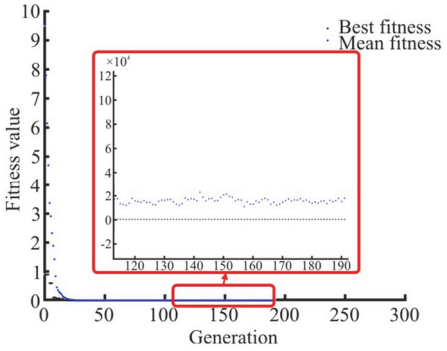

Fig. 2 (Color online) Convergence of GA

2. Optimization case of roll motion of box-shaped hull section with anti-rolling tanks and fins in beam wave

2.1 *Basic information of initial LNG tank*

In order to study the ship motion with multiple tanks in waves, especially the roll motion response of a ship under the condition of beam wave, the hull model is simplified in this paper to a certain degree, that is, the numerical simulation of the middle body section of a ship with double sloshing tanks is carried

out, which refers to the LNG liquid tank roll test conducted in the physical wave tank of Dalian University of Technology[21]. The main dimensions and installation components of the tank are shown in Fig. 3, in which the tank is fixed by a horizontal steel shaft, so that the tank can only rotate around the steel shaft. Other main parameters of the double liquid tank physical model are shown in Table 1.

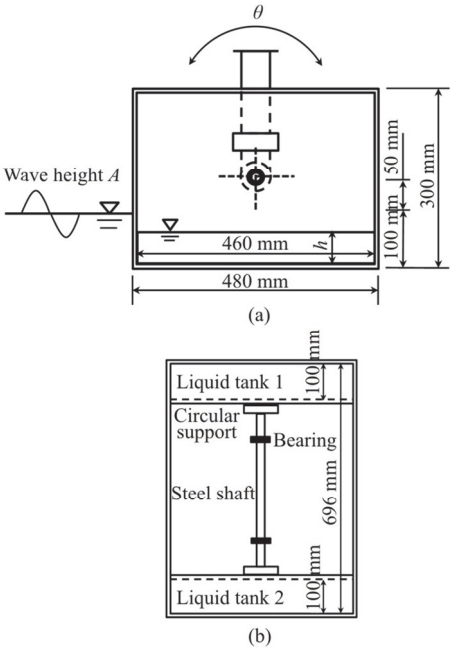

Fig. 3 The sketch and main dimension of the box-shaped hull section

Table 1 Main Particulars of the LNG tank

Parameters	Value
Tank mass (without liquid), M /kg	16.6
Moment of inertia for x axis, I_x /kg·m^2	0.419
Moment of inertia for z axis, I_z /kg·m^2	0.162
Tank natural frequency (without liquid), ω_n /rad·s^{-1}	5.536

2.2 *Verification of the numerical calculation of tank sloshing*

The viscous-flow-based CFD numerical simulation is carried out for the roll motion amplitude of the hull section model under the above condition. The size and boundary of the computational domain used in this case are shown in Fig. 4, and the specific boundary conditions are shown in Table 2. The mesh refinement is mainly concentrated around the hull section model and the free surface, and the global refinement of the computational domain is shown in Fig. 5.

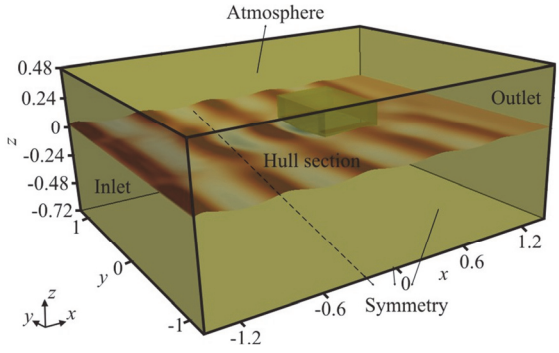

Fig. 4 (Color online) The size and boundaries of the computational domain

Table 2 Summary of boundary conditions

Boundary name	Boundary condition
Inlet	Velocity inlet (incident wave)
Atmosphere	No-slip
Hull section	No-slip wall
Symmetry	No-slip
Outlet	Pressure outlet

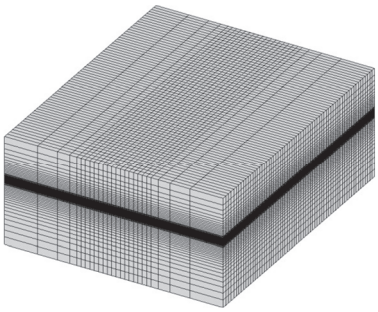

Fig. 5 Global refinement settings of the computational domain

To investigate the effect of roll motion with different filling ratio of the sloshing tank in internal-external flow coupling situation, several numerical simulations are set up at first while keeping the external excitation frequency and wave height (A = 0.03 m) of the beam waves constant. According to the numerical result [21] using the potential-flow-based method, compared with the model test result, a large deviation appears when the wave angular velocity is 6.7 rad/s, which is selected to be the wave angular velocity to verify the reliability of the numerical simulation method presented in this paper. Since the hull section model has two tanks, the two tanks can be filled separately. Five filling conditions are 0%-0% (case 1), 24.3%-0% (case 2), 38.3%-0% (case 3), 61.3%-0% (case 4) and 61.3%-61.3% (case 5) respectively.

Through numerical simulation, the roll motion amplitude of hull section under different liquid filling

ratios can be obtained, and the results are compared with the model test results, which are shown in Table 3.

Table 3 Comparison of dimensionless roll motion amplitude of liquid tanks with different filling ratios

Method	Dimensionless roll motion amplitude				
	Case 1	Case 2	Case 3	Case 4	Case 5
CFD	0.196	0.209	0.253	0.123	0.092
EFD	0.186	0.200	0.239	0.125	0.094
Relative error	4.85%	4.32%	5.65%	–1.74%	–2.07%

It can be seen from Table 3 that the relative error of the CFD simulation results in this paper is less than 6%, which indicates that the solver used in this paper can simulate the wave-induced sloshing tank problem with relatively high accuracy. Compared with the empty-tank condition, i.e., case 1, when the single-tank filling ratio is 24.3%, 38.3%, i.e., cases 2, 3, the roll motion amplitude of the tank increases, while when the single-tank or double-tank filling ratio is 61.3%, i.e., cases 4, 5, the roll motion amplitude of the tank decreases. To be specific, when the single-tank filling ratio is 38.3%, the natural sloshing frequency of the internal liquid is 6.63rad/s, which is close to the frequency of the incident wave, 6.7 rad/s. Therefore, the relatively strong sloshing phenomenon of the tank occurs.

For actual ships encountering waves, adding anti-rolling sloshing tanks can reduce ship motions to a certain extent, especially the roll motion when encountering beam waves. However, if the filling ratio of the liquid tank is too high, the ship displacement increases, and the total drag of the ship will probably increase, making the actual operating costs higher. In addition to setting anti-rolling tanks, anti-roll fins can also be installed on both sides of the ship to reduce its roll motion. Therefore, the filling ratio of the anti-rolling liquid tanks and the installation angle of the anti-rolling fins are considered to be optimized in this paper, so as to reduce the roll motion amplitude of the hull section to the greatest extent under the combined action of the two anti-rolling devices.

2.3 *Definition of the optimization problem*

For the roll motion response optimization of box-shaped hull section in beam wave, in order to further reduce the roll motion response, two anti-rolling fins are added on the outer surface of the hull section, with an initial installation angle of –45°, namely the free end downward slopes 45° from the horizontal plane, shown in Fig. 6.

The shape and size of the anti-rolling fin, hull section, and double liquid tank do not change during the process of optimization. On the contrary, the filling ratio of the double liquid tanks and the installation angle of the anti-rolling fin are changed during the optimization, whose design variables are the initial internal free surface coordinate in the vertical z-direction and the difference between the new and initial installation angles of anti-rolling fin α (counterclockwise) respectively, as shown in Fig. 7.

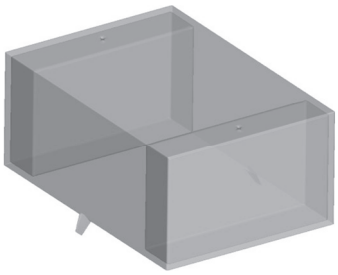

Fig. 6 The calculation model of the box-shaped hull section with fins

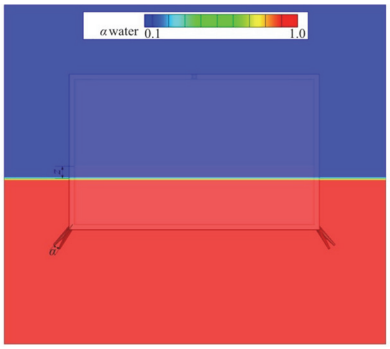

Fig. 7 (Color online) Schematic diagram of the two design variables

The specific value range of design variables is shown in Table 4. The OLHS method is used in two-dimensional design space for the design of experiment, and the sampling result is shown in Fig. 8.

Table 4 Design variables and their ranges

Design variable and unit	Lower bound	Upper bound
z /m	–0.03	0.03
α /°	–22.5	22.5

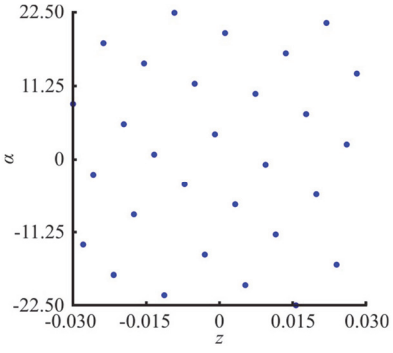

Fig. 8 (Color online) Sampling result of the design variables by OLHS method

New calculation cases are generated with computational grids similar to Fig. 5, but due to the existence of anti-rolling fin, additional local grid refinement is needed, as shown in Fig. 9, and the computational grids of the new samples are basically the same.

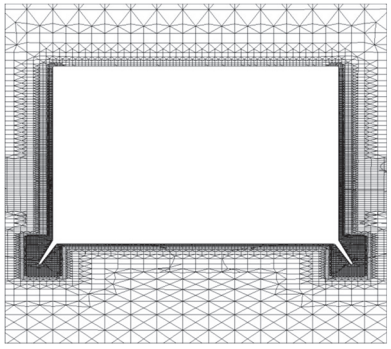

Fig. 9 Local grid refinement around the box-shaped hull section with anti-rolling fins

According to the Kriging model determined above, the single-objective GA is used to iteratively optimize the double-tank filling ratio and the variation angle of stabilizer fins. The main optimization parameters are listed in Table 5.

Table 5 Single-objective optimization parameters setup

Parameter	Value
Population size	200
Population iterations	800
Crossover rate	0.8
Mutation rate	0.2

The filling ratios of the initial and optimal liquid tanks and the shape comparison of hull sections are shown in Fig. 10. It can be seen that, under this beam wave, compared with the initial design, the filling ratio of the liquid tank is larger and the angle between the stabilizer fin and the horizontal plane is larger for the optimal design. The detailed values of design variables and the roll motion amplitude of hull section of the two designs are shown in Table 6.

Seen from Table 6, for the optimal design, the roll motion amplitude predicted by the constructed Kriging surrogate model is almost the same as the one evaluated by the actual viscous-flow CFD solver, with a relative error of only –0.4%, which indicates that the optimal design obtained by the Kriging model is reliable.

Figures 11, 12 show the internal-external fluid free surface elevation variations of the initial and optimal designs at typical moments in an encounter period under a given beam wave respectively. It can be obviously seen that, for the two designs, as the hull sections are at zero-speed speed, that is, in a floating state, under the action of the incident beam wave, the hull sections will do roll motion in the vicinity of the initial position, and the radiation wave occurs and superposes with the incident wave, making the external fluid near hull section (in the direction of incident wave) form an arc-shaped free surface elevation.

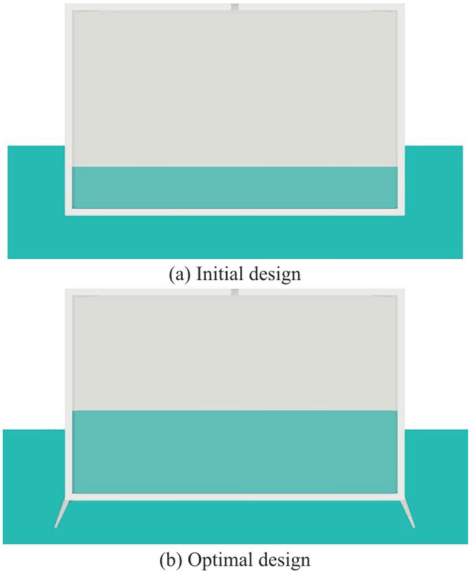

Fig. 10 (Color online) Comparison of the initial and optimal designs

Table 6 Summary of the optimal results, including design variables and objective functions

	Design variable value		Roll motion amplitude φ /°		
	z /m	θ /°	Kriging	CFD	Drop percent
Initial	–0.0299	-	-	0.2559	-
Optimal	0.0265	–22.5	0.2487	0.2498	2.4%

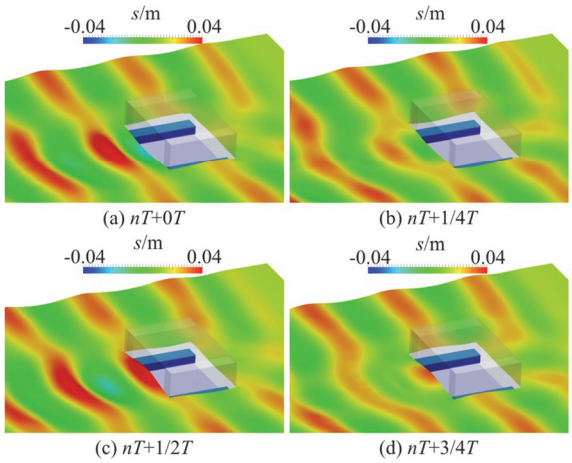

Fig. 11 (Color online) Free surface wave elevations of the initial design

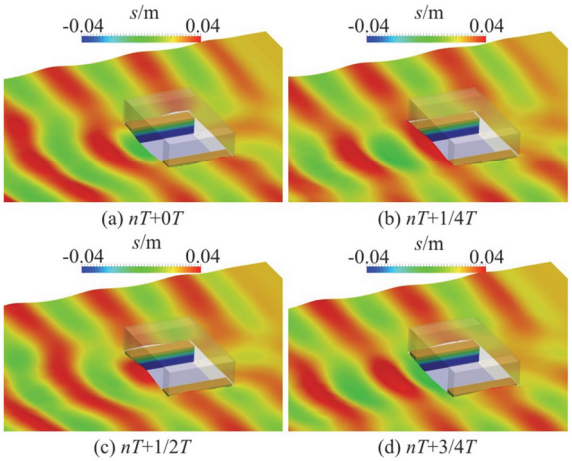

Fig. 12 (Color online) Free surface wave elevations of the optimal design

For the initial design, compared with the optimal design, the front of the hull section (in the direction of incident wave) has larger wave climbing and sag, indicating that the initial design has a larger roll motion amplitude. In addition, shown in Figs. 11, 12 with the same color bar of the free surface wave elevation, the free surface wave elevation of the initial design is relatively small, which is caused by the superposition of the larger radiation wave generated by the larger roll motion of the hull section and the incident beam wave. On the contrary, the optimal design has a smaller roll motion, resulting in a smaller radiation wave generated, which makes the superposition degree of the two waves smaller, so the shape (wave height) of the incident wave keeps better than that in the initial case. As for the internal flow in the liquid tanks, the free surface movement in the tanks of the initial design is larger than that of the optimal design. As a matter of fact, the free surface movement of the tanks of the two designs is not very obvious, which is shown as the overall shaking of the free surface in the tank carrying the liquid below the free surface. In conclusion, for the optimal design, the double-tank with a filling ratio of 37.6% inhibits the roll motion of the box-shaped hull section.

Finally, the similarities and differences between the two designs are analyzed from the perspective of the flow field near the stabilizer fins. Figures 13, 14 show the variations of the vorticity[22] distribution near hull of the initial and optimal designs at typical moments in an encounter period under a given beam wave respectively. Seen from Figs. 13, 14, for the two designs, the incident beam wave is weakened after the floating hull section, especially at the rear of hull section (in the direction of incident wave), so the free surface wave elevation has a significantly difference before and after the hull section. Furthermore, as a result of the wave propagation, certain vorticity near the free surface will produce.

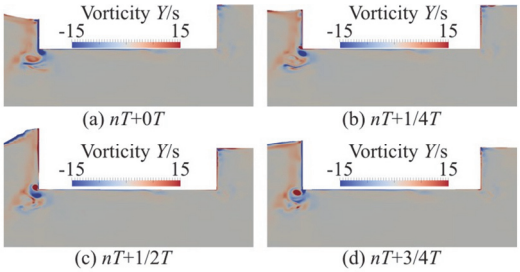

Fig. 13 (Color online) Vorticity distribution at the central longitudinal plane of the hull section of initial design near hull

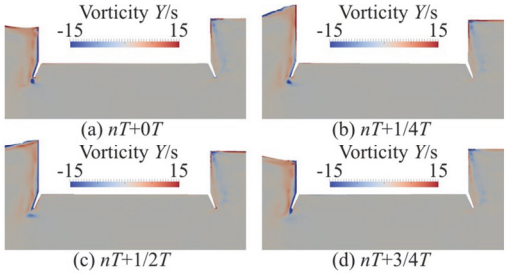

Fig. 14 (Color online) Vorticity distribution at the central longitudinal plane of the hull section of optimal design near hull

Due to the roll motion of the hull section, vorticity is also generated near the corner point, as shown in the lower left corner of the hull section in Figs. 13, 14. Therefore, a certain viscous damping is formed and a stabilizing moment is generated, thus inhibiting the roll motion of the hull section. For the optimal design, however, due to the installation of the fin stabilizer, the vorticity distribution and intensity near corner point is changed, compared with the original design. In particular, alternating leakage vortex occurs near the free end of the anti-rolling fin, which are basically negative vortex in contrast to the roll motion. Therefore, additional stabilizing moment arises, making the roll motion of hull section decreased. In conclusion, for the optimal design, the stabilizer fin at the installation angle –67.5° also inhibits the roll motion of the box-shaped hull section.

3. Conclusions

The internal-external coupling flow effect is vital for the ship and liquid tank designs, especially when the external wave frequency is close to the natural frequency of liquid tanks with a certain filling ratio, large amplitude motions may occur, which is dangerous to some extent. After introducing the widely-used simulation-based-design method in the field of ship

and offshore structure hydrodynamic performance optimization, and the verification of the numerical calculation of tank sloshing is then done, indicating that the solver used in this paper can simulate the wave-induced sloshing tank problem with relatively high accuracy. Specifically, when the single-tank filling ratio is 38.3%, the natural sloshing frequency of the internal liquid is close to the frequency of the incident wave, so the relatively strong sloshing phenomenon of the tank occurs.

For actual ships encountering waves, adding anti-rolling sloshing tanks can reduce ship motions to a certain extent, especially the roll motion when encountering beam waves. Furthermore, anti-roll fins can also be installed on both sides of the ship to reduce its roll motion by generating stabilizing moment. In this paper, the filling ratio of the anti-rolling liquid tank and the installation angle of the anti-rolling fins of the box-shaped hull section are optimized, in order to reduce the roll motion amplitude of the hull section to the greatest extent under the combined action of the two anti-rolling devices.

The surrogate-model-based optimization is finally done to obtain the optimal combination of the filling ratio of the anti-rolling liquid tank and the installation angle of the anti-rolling fins, which reach a 2.4% decrease for the roll motion amplitude of the hull section in a typical beam wave. From further evaluation, it can be seen that the optimal filling ratio causes a deviation of the natural sloshing frequency of the internal liquid and the incident wave, and the optimal installation angle of the anti-rolling fins can generate larger vorticity near the hull section, resulting in the generation of an extra stabilizing moment.

To sum up, results show that the roll motion amplitude of box-shaped hull section can be successfully reduced by optimizing the two anti-rolling devices, which can be a reference to the future designs and optimizations of the fishing ship, in order to avoid the fish in the liquid tank be rocked to death due to the ship roll motion in waves, and other kinds of ships with anti-rolling liquid tank or fins.

References

[1] Mikelis N. E., Miller J. K., Taylor K. V. Sloshing in partially filled liquid tanks and its effect on ship motions: Numerical simulations and experimental verification [C]. *Royal Institution of Naval Architects Spring Meeting*, London, UK, 1984, 267-281.

[2] Rognebakke O. F., Faltinsen O. M. Coupling of sloshing and ship motions [J]. *Journal of Ship Research*, 2003, 47(3): 208-221.

[3] Newman J. N. Wave effects on vessels with internal tanks [C]. *20th Workshop on Water Waves and Floating Bodies*, Spitsbergen, Norway, 2005.

[4] Akyildiz H. A numerical study of the effects of the vertical baffle on liquid sloshing in two-dimensional rectangular tank [J]. *Journal of Sound and Vibration*, 2012, 331(1): 41-52.

[5] Jiang S. C., Teng B., Bai W. et al. Numerical simulation of coupling effect between ship motion and liquid sloshing under wave action [J]. *Ocean Engineering*, 2015, 108: 140-154.

[6] Saripilli J. R., Sen D. Numerical studies of coupling effect of sloshing on 3D ship motions [J]. *International Journal of Offshore and Polar Engineering*, 2017, 27(1): 27-35.

[7] Shen Z., Wan D. Numerical simulations of large-amplitude motions of KVLCC2 with tank liquid sloshing in waves [C]. *2nd International Conference Violent Flows*, Nantes, France, 2012, 149-156.

[8] Hirt C. W., Nichols B. D. Volume of fluid (VOF) method for the dynamics of free boundaries [J]. *Journal of Computational Physics*, 1981, 39(1): 201-225.

[9] Larsen J., Dancy H. Open boundaries in short wave simulations–A new approach [J]. *Coastal Engineering*, 1983, 7(3): 285-297.

[10] Cao H. J., Wan D. C. Three-dimensional numerical wave tank based on naoe-FOAM-SJTU [J]. *Journal of Fudan University (Natural Science)*, 2013, 5: 627-634.

[11] Zhuang Y., Wan D. C. Parametric study of a new HOS-CFD coupling method [J]. *Journal of Hydrodynamics*, 2021, 33(1): 43-54.

[12] McKay M. D., Beckman R. J., Conover W. J. Comparison of three methods for selecting values of input variables in the analysis of output from a computer code [J]. *Technometrics*, 1979, 21(2): 239-245.

[13] Liu X. W., Wan D. C. Hull form optimization of wave-making resistance in different speeds for a luxury cruise ship [J]. *Chinese Journal of Ship Research*, 2020, 15(5): 1-10, 40.

[14] Sobol I. On the systematic search in a hypercube [J]. *SIAM Journal on Numerical Analysis*, 1979, 16(5): 790-793.

[15] Krige D. G. A statistical approach to some basic mine valuetion problems on the Witwatersrand [J]. *Journal of the Chemical, Metallurgical and Mining Engineering Society of South Africa*, 1951, 52(6): 119-139.

[16] Box G. E. P., Wilson K. B. On the experimental attainment of optimum conditions [J]. *Journal of the Royal Statistical Society, Series B*, 1951, 13(1): 1-45.

[17] Smith M. Neural networks for statistical modeling [M]. New York, USA: Von Nostrand Reinhold, 1993.

[18] Goldberg D. E. Genetic algorithms in search, optimization, and machine learning [M]. New York, USA: Addison-Wesley Publishing Company, 1989.

[19] Kennedy J., Eberhart R. Particle swarm optimization [C]. *International Conference on Neural Networks*, Perth, WA, Australia, 2002, 1942-1948.

[20] Ackley D. H. An empirical study of bit vector function optimization [C]. *Genetic Algorithms and Simulated Annealing Conference*, London, UK, 1987, 171-204.

[21] Jiang S. C. Numerical simulation on coupled effect between ship motion and liquid sloshing under wave action [D]. Doctoral Thesis, Dalian, China: Dalian University of Technology, 2013(in Chinese).

[22] Liu X. W., Chen S. T., Zhao W. W. et al. Liutex-based centripetal force field model for improving the resistance and wake performances of JBC ship sailing in calm water [J]. *Journal of Hydrodynamics*, 2021, 33(3): 494-502.